HHS Public Access

Author manuscript

Toxicology. Author manuscript; available in PMC 2016 July 03.

Published in final edited form as:

Toxicology. 2015 July 3; 333: 25–36. doi:10.1016/j.tox.2015.03.008.

Effects of nitrogen-doped multi-walled carbon nanotubes compared to pristine multi-walled carbon nanotubes on human small airway epithelial cells

Amy L. Mihalchik[a,c], **Weiqiang Ding**[b], **Dale W. Porter**[c], **Colleen McLoughlin**[c], **Diane Schwegler-Berry**[c], **Jennifer D. Sisler**[c], **Aleksandr B. Stefaniak**[d], **Brandi N. Snyder-Talkington**[c], **Rodolfo Cruz-Silva**[e], **Mauricio Terrones**[e,f], **Shuji Tsuruoka**[e], **Morinobu Endo**[e], **Vincent Castranova**[a], and **Yong Qian**[c,*]

[a] Pharmaceutical and Pharmacological Sciences, West Virginia University School of Pharmacy, Morgantown, WV 26505, United States

[b] Shared Research Facilities, West Virginia University, Morgantown, WV 26505, United States

[c] Pathology and Physiology Research Branch, Health Effects Laboratory Division, National Institute for Occupational Safety and Health, Morgantown, WV 26505, United States

[d] Division of Respiratory Disease Studies, National Institute for Occupational Safety and Health, Morgantown, WV 26505, United States

[e] Research Center for Exotic Nanocarbons, Shinshu University, Nagano, Japan

[f] Departments of Physics, Chemistry, Materials Science & Engineering, and Center for 2-Dimensional and Layered Materials, The Pennsylvania State University, University Park, PA 16802, United States

Abstract

Nitrogen-doped multi-walled carbon nanotubes (ND-MWCNTs) are modified multi-walled carbon nanotubes (MWCNTs) with enhanced electrical properties that are used in a variety of applications, including fuel cells and sensors; however, the mode of toxic action of ND-MWCNT has yet to be fully elucidated. In the present study, we compared the interaction of ND-MWCNT or pristine MWCNT-7 with human small airway epithelial cells (SAEC) and evaluated their subsequent bioactive effects. Transmission electron microscopy, X-ray photoelectron spectroscopy, Raman spectroscopy, and X-ray diffraction suggested the presence of N-containing defects in the lattice of the nanotube. The ND-MWCNTs were determined to be 93.3% carbon, 3.8% oxygen, and 2.9% nitrogen. A dose–response cell proliferation assay showed that low doses

* Corresponding author at: NIOSH, HELD, PPRB, 1095 Willowdale Dr., Morgan-town, WV 26505, United States. Tel.: +1 304 285 6286. yaq2@cdc.gov (Y. Qian)..

Disclaimer

The findings and conclusions in this report are those of the authors and do not necessarily represent the views of the National Institute for Occupational Safety and Health. The mention of Mitsui & Co., Ltd. and MWCNT-7 does not constitute product endorsement.

Conflict of interest

The authors declare that there are no conflicts of interest.

Transparency document

The Transparency document associated with this article can be found in the online version.

of ND-MWCNT (1.2 mg/ml) or MWCNT-7 (0.1 mg/ml) increased cellular proliferation, while the highest dose of 120 mg/ml of either material decreased proliferation. ND-MWCNT and MWCNT-7 appeared to interact with SAEC at 6 h and were internalized by 24 h. ROS were elevated at 6 and 24 h in ND-MWCNT exposed cells, but only at 6 h in MWCNT-7 exposed cells. Significant alterations to the cell cycle were observed in SAEC exposed to either 1.2 mg/ml of ND-MWCNT or MWCNT-7 in a time and material-dependent manner, possibly suggesting potential damage or alterations to cell cycle machinery. Our results indicate that ND-MWCNT induce effects in SAEC over a time and dose-related manner which differ from MWCNT-7. Therefore, the physicochemical characteristics of the materials appear to alter their biological effects.

Keywords

Multi-walled carbon nanotubes; Functionalized multi-walled carbon; nanotubes; Reactive oxygen species

1. Introduction

As the field of nanotoxicology rapidly expands, researchers are working towards the identification of key toxicity parameters that can be applied across materials. Since their introduction, multi-walled carbon nanotubes (MWCNT) have been used in a wide variety of industrial applications due to their unique physico-chemical properties; however, these unique characteristics may pose a threat to workers and the public during production, use, and disposal (NIOSH, 2013; Oberlin et al., 1976). The high aspect ratio, surface characteristics, durability, and redox potential of MWCNT contribute to their bioactivity, therefore suggesting potential routes for improving their safety profile. (NIOSH, 2013). Pristine MWCNT (including MWCNT-7) have been shown in numerous studies to induce acute inflammatory and chronic fibrogenic responses both *in vitro* and *in vivo* (Kasai et al., 2014; Mercer et al., 2011; Pacurari et al., 2011; Porter et al., 2010; Snyder-Talkington et al., 2013a). In order to improve MWCNT safety and biocompati-bility, material scientists have begun implementing “safety by design” practices in the synthesis of carbon nanotubes (CNT) with alternative physicochemical properties. With this in mind, next-generation MWCNT may be more or less toxic compared to their first generation counterparts and may cause toxicity through alternative mechanisms.

MWCNT-7 have been shown to induce inflammation and fibrosis *in vivo* at occupationally relevant doses in mice and rats (Mercer et al., 2010, 2013; Porter et al., 2010, 2013). At an inhalation exposure of 5 mg/m^3, MWCNT-7 were capable of bypassing the defenses of the mouse lung due to their small size, with approximately 84% of the MWCNT-7 found in the alveolar region one day post-exposure (Mercer et al., 2011). In a 2010 study, Porter et al. showed that mice exposed to 10, 20, 40 or 80 mg of pristine MWCNT-7 exhibited short-term polymorphonuclear leukocyte infiltration and lactate dehydrogenase release, and pulmonary fibrosis at 7 days post-exposure. A recent inhalation study in mice suggests that MWCNT-7 are biopersistent, can remain in the lung, and may travel throughout the periphery approximately one year post-exposure (Mercer et al., 2013).

A review of MWCNT *in vitro* studies indicated that exposures up to 200 mg/ml of MWCNT are commonly used which are irrelavent to doses achieved within the mouse and human lung (Snyder-Talkington et al., 2012). However, some *in vitro* studies utilize lower exposures ranging from 0.1 mg/mL to 6 mg/mL that further support the *in vivo* results, suggesting that pristine MWCNT, including MWCNT-7, are capable of inducing molecular signals potentially responsible for the toxic effects observed *in vivo* (Ding et al., 2005; Pacurari et al., 2012; Mishra et al., 2012; Snyder-Talkington et al., 2013a,b,c; Wang et al., 2014). In this study, the dosage of 1.2 mg/ml of MWCNT-7 or ND-MWCNT was selected to be reflective of previously conducted *in vivo* studies, roughly correlating with a 60 mg dose of MWCNT in mice based upon the alveolar surface area of the mouse lung and surface area of a cell culture dish (Porter et al., 2010). These *in vivo* doses were roughly reflective of lung burdens due to concentrations of airborne MWCNT measured in actual workplaces and account for MWCNT mass median aerodynamic diameter, minute ventilation, and human alveolar epithelium surface area (Han et al., 2008; Snyder-Talkington et al., 2012).

The addition of defects or heteroatoms, such as nitrogen, to MWCNT can change their crystallinity and reactivity for industrial use, and may also impact their bioactivity. ND-MWCNT have been synthesized using a variety of starting materials, catalysts, and methods, resulting in CNT with varying percentages of nitrogen and levels of disruption to the graphene lattice. ND-MWCNT are suspected to grow by a base-growth model limited by diffusion of carbon atoms toward the catalyst molecules, coverage of the catalyst sites by amorphous carbon, or constraints brought on by pyridinic N-incorporation (Sharifi et al., 2012; Terrones et al., 2002). N-incorporation can be pyridinic (sp^2 coordinated, N atom part of hexagon ring connecting two C atoms) or pyrrolic (sp^3 coordinated, N atom part of pentagon ring connecting two C atoms) depending on the percentage of nitrogen in the CNT and the doping conditions. Therefore, since ND-MWCNT fabrication is not standardized, physicochemical characterization is of great importance for understanding their biological effects and potential toxicities.

Traditional pristine MWCNT have limited electrical conductance compared to doped variants; however, the addition of nitrogen to the carbon lattice confers MWCNT n-type semiconductor properties (Ayala et al., 2010). ND-MWCNT typically lack a hollow core common to pristine MWCNT and have bamboo-like sections walled off by layers of graphene. Nitrogen creates defects in the MWCNT by forcing rearrangement of the carbons around the heteroatoms, thereby introducing disorder into the graphene layers and curvature of the CNT (Ayala et al., 2010). Since nitrogen has one additional electron as compared to carbon, it is believed that this extra electron can carry current and also potentially interact with ROS, which are highly unstable radicals containing at least one oxygen atom. Tsuruoka et al. (2013a) suggested that unpaired electrons on the surface of MWCNT may participate in reactions with ROS. They assessed a variety of MWCNT with different modifications for ROS quenching through electron spin resonance studies, and showed that doping and surface chemistry altered the ability of CNT to quench ROS. The ability to produce ROS is a key characteristic of MWCNT that can be controlled by surface modification and composition and directly alters MWCNT-induced potential toxicity in biological systems

(Tsuruoka et al., 2013b). Addition of functional groups to the surface of MWCNT, such as nitrogen groups, carboxyl groups, polyethelene glycol, or others, can also alter the uptake and biocompatibility of MWCNT as recently shown by Li et al. (2013).

ND-MWCNT are used in a variety of applications including gas sensors, matrix fillers in composite materials, field emission devices, and improved lithium storage in lithium batteries; however, information on ND-MWCNT bioactivity is limited (Ayala et al., 2010). Carrero-Sanchez et al. (2006) showed that ND-MWCNT (2–4% nitrogen) are associated with lesser toxicities and pathological conditions compared to pristine CNT in an *in vivo* rat model after nasal, oral, intratracheal, and intraperitoneal exposures up to 5 mg/kg. Only the highest dose (5 mg/kg) led to hyperplasia, inflammatory cell infiltration, fibroblastic proliferation, and some granulomas in ND-MWCNT treated rats, but was lethal in pristine CNT-exposed animals. Limited *in vitro* results suggest their biocompatibility with blood cells with minimal toxicity at higher doses (20 mg/ml), which could be useful for potential intravenous drug delivery (Zhao et al., 2011). Elías et al. (2007) have also demonstrated that ND-MWCNT are the only type of CNT tested that do not reduce cell viability in amoeba (even at higher doses), thus indicating that these N-doped CNTare less toxic when compared to other types. However, others have shown that tube length may play a key role in toxicity, with longer ND-MWCNT being more toxic than other functionalized CNT (Boncel et al., 2011).

The present study assessed the bioactivity of ND-MWCNT and MWCNT-7 at low exposures in h-TERT immortalized human small airway epithelial cells (SAEC) derived from the lower bronchioles. Through assessment of physical characteristics, uptake into SAEC, cell viability, ROS production, and cell cycle analysis, we provide an *in vitro* benchmark for ND-MWCNT toxicity as compared to MWCNT-7 in a model of lung epithelium.

2. Materials and methods

2.1. D-MWCNT and MWCNT-7

The ND-MWCNT used in this study were a gift from Mauricio Terrones (Pennsylvania State University, University Park, PA), and Morinobu Endo, and Shuji Tsuruoka (Shinshu University, Nagano, Japan). ND-MWCNT were characterized at the Morgantown National Institute for Occupational Safety and Health and West Virginia University Shared Research Facilities. The MWCNT-7 used in this study were originally obtained through the Mitsui & Co., Ltd. (MWCNT-7, lot #05072001K28) and previously characterized (Porter et al., 2010).

2.2. ND-MWCNT and MWCNT-7 preparation

For cell culture studies, ND-MWCNT were prepared in dispersion media (DM) consisting of PBS (pH 7.4, Ca/Mg-free) supplemented with 0.6 mg/ml mouse serum albumin and 1.1 mg/ml 1,2-dipalmitoyl-sn-glycero-3-phosphocholine (DPPC) as previously described (Porter et al., 2008). DPPC was prepared fresh as a 1 mg/ml stock solution in 100% ethanol. Transmission electron microscopy (TEM) micrographs of MWCNT dispersed in DM demonstrated that DM promotes significant dispersion of MWCNT (Porter et al., 2008).

ND-MWCNT and MWCNT-7 were prepared in DM by indirect sonication at 4 °C for 5 min (Hielscher ultrasonic processor, UIS259L; Ringwood, NJ) at amplitude 100% and cycle 1. Following indirect sonication, the suspension was directly sonicated for 5 min at 5 W output and 30% duty cycle in 1 min increments (Branson Sonifier 450; Danbury, CT). The stock solution (0.5 mg/ml) of ND-MWCNT or MWCNT-7 was kept at 4 °C and used within 2–3 weeks. The ND-MWCNT and MWCNT-7 stock solutions were directly sonicated for 1 min at 5 W output and 30% duty cycle prior to cell culture experiments. Cells were treated with DM, ND-MWCNT, or MWCNT-7 at 1.2 mg/ml, a concentration which was extrapolated from previous murine *in vivo* exposure experiments based upon alveolar surface area (Porter et al., 2010).

2.3. Cell culture

SAEC were a gift from Tom K. Hei (Columbia University, New York, NY) (Piao et al., 2005). SAEC were cultured in serum-free SABM medium supplemented with a SAGM SingleQuot kit of growth factors, cytokines, and supplements (Lonza Walkersville, Inc., Walkersville, MD). SAEC were maintained in an incubator at 37 ° C with 5% CO_2. For cell culture experiments, SAEC were serum starved 24 h prior to ND-MWCNT or MWCNT-7 exposure in serum-free SABM medium.

2.4. Transmission electron microscopy (TEM)

Samples of ND-MWCNT were diluted in double distilled H_2O (ddH_2O) followed by vortexing, and a drop of solution was placed on a formvar-coated copper grid and allowed to air dry. Images were photographed under a JEOL 1220 transmission electron microscope (Peabody, MA). Additionally, SAEC interaction with and engulfment of ND-MWCNT and MWCNT-7 were then analyzed by TEM. SAEC were grown to confluence and exposed to 1.2 mg/ml DM, ND-MWCNT, or MWCNT-7 for 6 or 24 h. Cells were trypsinized with ReagentPack Subculturing reagents (Lonza Walkersville, Inc., Walkersville, MD) per manufacturer guidelines and harvested by centrifugation at 400 x g for 5 min. Cells were fixed in Karnovksy's fixative (2.5% glutaraldehyde and 3% paraformaldehyde in 0.1 M sodium cacodylate, pH 7.4), washed three times in 0.1 M sodium cacodylate, and postfixed in 1% osmium tetraoxide, followed by washing with 0.1 M sodium cacodylate and distilled water. The cells were dehydrated by sequential washings in 25, 50, and 100% ethanol and embedded in LX-112 (Ladd, Williston, VT). Ultrathin sections were stained with uranyl acetate and lead citrate and examined with a JEOL 1220 transmission electron microscope.

2.5. Field emission scanning electron microscopy (FESEM)

The particles were dispersed in ddH_2O and filtered with a 0.2 mm nucleopore filter. The filter was attached with double-stick carbon tape on an aluminum mount and sputter coated with gold/palladium. Images were collected on a Hitachi (Tokyo, Japan) S-4800 field emission scanning electron microscope.

2.6. X-ray photoelectron spectroscopy (XPS)

XPS analysis was carried out with a Physical Electronics VersaProbe 5000 XPS (Chanhassen, MN). ND-MWCNT powder was pressed into a small pellet and evacuated in

an entry chamber for approximately 2 h before being transferred to an ultra-high vacuum chamber for analysis. The sample was stimulated by a focused aluminum K-a X-ray source at 1486 eV energy and 25 W power with an X-ray spot size of 100 mm. A survey scan was carried out using an analyzer pass energy of 117.40 eV, and high-resolution scans for carbon, oxygen, and nitrogen elements were carried out at an analyzer pass energy of 23.50 eV. The spectra were referenced to the C1s peak at a binding energy of 284.8 eV.

2.7. Raman spectroscopy

Raman spectra of the MWCNT were collected using a Renshaw Invia Raman spectrometer with a CCD detector (Hoffman Estates, IL). ND-MWCNT or MWCNT-7 powders were directly placed on a microscope glass slide, which was then mounted under the 50x objective lens of the Raman microscope. Samples were excited with a 532 nm green laser at around 0.23 mW laser power for data collection.

2.8. X-Ray diffraction (XRD)

XRD patterns of the MWCNT were collected with a PANana-lytical X'Pert Pro powder X-ray diffractometer. ND-MWCNT or MWCNT-7 powders were filled into stainless steel powder sample holders and radiated with a Cu K-a X-ray source at 1.8 kW power in a theta/theta scan mode. The XRD spectra of the samples were collected over a 2-theta range of 15–90° at a step size of 0.05° with a solid state X-ray detector.

2.9. Zeta potentials

The electrophoretic mobility (motion of particles relative to a fluid under the influence of an electric field) of particles was determined using light scattering in an applied electric field and converted to values of zeta potential (the potential difference between a dispersion medium and stationary layer of uid attached to a particle in the medium) using the Henry equation. For each material, an independent sample was drawn for determination of electrophoretic mobility. The instrument operability was previously verified using U.S. National Institute of Standards and Technology Standard Reference Material 1980: Positive Electrophoretic Mobility, having a certified value for mobility of 2.53 ± 0.12 mm cm/(V s), corresponding zeta potential of ~32.5 mV at 25 °C, and prepared using the protocol described in the SRM certificate. The pH of the experimental samples was determined after measurement of electrophoretic mobility using a calibrated electrode attached to a volt meter. The pH probe tip was rinsed thoroughly with 18 MV cm ddH_2O and blotted dry before measurements. The PBS had a pH of 7.2, and SAEC serum-free media had a pH of 7.6. The parameters for the dispersants were based on PBS (refractive index = 1.334, viscosity = 0.9110 cP, dielectric constant = 79.0, and Smoluchowski approximation, f(ka) value = 1.5). Zeta potential is used as an indicator of the stability characteristics of a dispersion. Riddick (1968) developed categories to describe the stability of dispersions based on zeta potential: threshold of agglomeration (−10 to −15 mV), threshold of delicate dispersion (−16 to −30 mV), moderate stability (−31 to −41 mV), fairly good stability (−41 to −60 mV), and very good stability (−61 to −80 mV). All measurements were performed at 25 ° C using a Malvern Zetasizer Nano ZS90 (Worcestershire, UK) equipped with a 633 nm laser at a 90° scattering angle. Samples were equilibrated inside the instrument for 2 min,

and five measurements (10 s delay between measurements), each consisting of five runs (2 s delay between runs), were recorded.

2.10. ROS production

ROS measurements by confocal microscopy were performed according to methods previously described (Qian et al., 2010). SAEC were cultured on glass cover slips, serum starved 24 h, and exposed to 1.2 mg/ml DM, ND-MWCNT, or MWCNT-7 for 6 or 24 h. Dihydroethidium (DHE) (Sigma–Aldrich, St. Louis, MO) was added at a final concentration of 5 mM for the last 30 min of exposure in the dark. After incubation, cells were washed twice with PBS (pH 7.4), fixed with 4% paraformaldehyde, washed three times over 15 min with PBS, and mounted on slides with ProLong Gold anti-fade (Invitrogen; Carlsbad, CA). A Zeiss LSM 510 microscope was used to obtain images with a 20x objective. DHE staining was determined by fluorescence at 546 nm. Five independent experiments were carried out with representative images taken from each slide. Images from a single experiment overall reflective of these experiments are found in Fig. 7.

2.11. Cell proliferation assay

A dose–response assessment of cellular proliferation was carried out by seeding SAEC (1 $x10^4$ cells) in 100 ml complete media in 96-well plates, followed by 24 h serum starvation prior to exposure to DM, ND-MWCNT, or MWCNT-7 for 24 h at 0, 0.12, 1.2, 12, or 120 mg/ml. Twenty microliters of CellTiter 96® Aqueous One Solution (Promega; Madison, WI) was added to each well during the last 4 h of exposure. Absorbance was read at 490 nm using a BioTek Synergy H1 plate reader (Winooski, VT), and statistical analyses were carried out using the Data Analysis pack in Microsoft Excel (Redmond, WA). Three experiments were performed in triplicate; treatment groups were averaged by triplicate and compared using two sample t-tests assuming unequal variances. Error bars are reflective of standard error.

2.12. Cell cycle assessment

SAEC were grown to subconfluency, serum starved for 24 h, and treated with 1.2 mg/ml DM, MWCNT-7, or ND-MWCNT. Cells were collected by trypsinization, followed by centrifugation at 1100 x g for 7 min. Cell pellets were washed in PBS and subsequently resuspended in 100 mL PBS. Cells were fixed in 70% ethanol and stored at 4 ° C until assessed by flow cytometry. Fixed SAEC were centrifuged and washed twice with PBS, treated with 50 mL of 100 mg/ml RNase (Sigma–Aldrich, St. Louis, MO), and stained with a final concentration of 10 mg/ml propidium iodide (Sigma– Aldrich, St. Louis, MO). Samples were run on an LSRII cell analyzer (BD Biosciences, San Jose, CA). Ten thousand events were collected per sample, and analysis was carried out using FlowJo software (Ashland, OR). Gating was set to exclude debris and only include cells by forward and side scatter. Gating for singlet discrimination was through pulse width *versus* area for phycoerythrin, forward scatter, and side scatter. The Watson model was used to determine the percentage of cells in each phase. Cells in each phase were analyzed from two independent trials in biological triplicate ($n = 6$) from which 10,000 events were collected from each individual sample. Statistical analysis was done using the Data Analysis pack in

Microsoft Excel (Redmond, WA). Treatment groups were compared using two sample t-tests assuming unequal variances and error is presented as standard error in Table 2.

2.13. Western blotting

Whole cell protein extraction was carried out using RIPA buffer (150 mM NaCl, 10 mM Tris pH 7.4, 2 mM EDTA, 1% IGEPAL, 1% sodium deoxycholate, 0.1% sodium dodecyl sulfate) supplemented with a 10 mg/ml protease inhibitor cocktail and 10 mg/ml phosphatase inhibitor (Thermo Fisher Scientific, Waltham, MA). Protein concentration was measured using a BCA protein assay kit (Thermo Fisher Scientific, Waltham, MA). Twenty micrograms of protein per sample was resolved using sodium dodecyl sulfate-polyacrylamide gel electrophoresis (SDS-PAGE) and transferred to polyvinylidene fluoride membranes (PVDF, Pall Corporation; Pensacola, FL). Membranes were blocked for 1 h in 5% bovine serum albumin (Thermo Fisher Scientific, Waltham, MA) in Tris buffered saline with Tween-20 (TBST) (62.5 mM Tris pH 7.4, 150 mM NaCl, 0.05% Tween 20) (Thermo Fisher Scientific, Waltham, MA) and incubated with CDK4, phospho-tyrosine, or phospho-threonine (Cell Signaling Technology, Boston, MA) primary antibodies overnight at 4 ° C. Membranes were washed three times with TBST for 10 min each and incubated with species-specific secondary antibodies for 1 h at room temperature. Analysis was carried out using ECL Western Blotting Substrate (Thermo Fisher Scientific, Waltham, MA). Representative western blots are shown in Figs. 8 and 9 from a minimum of three independent experiments per antibody. Densitometry was carried out using ImageJ software (NIH, Bethesda, MD) on three representative western blots normalized to respective b-actin blots per antibody. Error bars in the bar graphs show standard error.

3. Results

3.1. Characteristics of ND-MWCNT and MWCNT-7 in suspension

Low magnification TEM (Fig. 1A, B) and FESEM (Fig. 1C, D) indicated that the ND-MWCNT were 5.28 ± 2.07 mm long and 79.7 ± 19.4 nm wide, after assessment for size in Adobe Photoshop CS5 (San Jose, CA). The ruler tool was used to measure single nanotubes from the TEM and SEM images. As previously determined, the MWCNT-7 were determined to be 3.86 (GSD 1.94) mm long and 49 ± 13.4 nm wide (Porter et al., 2010) (Table 1). Zeta potentials were measured for ND-MWCNT and MWCNT-7 in DM diluted in PBS and serum free SAEC media. In PBS (pH 7.2), values were determined to be -13.9 ± 0.485 mV and -15.8 ± 0.450 mV, respectively. In serum free media (pH 7.6), values were determined to be -12.9 ± 0.835 mV and -12.2 ± 0.283 mV, respectively (Table 1), and there was no appreciable difference in zeta potentials between particles in PBS and those in serum free SAEC media.

3.2. Physical characteristics of ND-MWCNT and MWCNT-7

Several analytic methods were used to assess the physical characteristics of the ND-MWCNT and MWCNT-7, including XPS, Raman spectroscopy, and XRD. The MWCNT-7 were previously characterized by Porter et al. (2010) as pristine MWCNT with 20–50 walls per nanotube and with minimal trace metal contamination, including sodium (0.41%) and iron (0.32%). XPS determined the elemental composition and surface chemistry of the ND-

MWCNT. The XPS survey scan revealed the existence of carbon, oxygen, and nitrogen elements within ND-MWCNT. The corresponding atomic concentration was determined from high resolution spectra of carbon, oxygen, and nitrogen elements, showing that the ND-MWCNT were composed of approximately 93.3% carbon, 3.8% oxygen and 2.9% nitrogen (Fig. 2A). The spectra of these elements were analyzed, and different chemical states were identified. The carbon atoms were found to be in three functional groups: sp^2-hybridized graphitic carbon (284.8 eV), C–N (285.9 eV), and C=O (287.3 eV) (Fig. 2B). The nitrogen atoms were found to be in two chemical states: amino $–NH_2$ (399.0 eV) and pyrrolic C–N (400.3 eV) types (Seran et al., 2012; Zhang et al., 2013) (Fig. 2D). The oxygen atoms were found to be in two chemical states: C=O (531.8 eV) and –OH (533.6 eV) (Fig. 2C). These XPS results further showed the inclusion of nitrogen atoms into the graphitic carbon lattice of ND-MWCNT (pyrrolic C–N bonding) and the existence of lattice structural disorder.

To further characterize these materials, Raman spectroscopy was used to assess the carbon lattice structure condition of ND-MWCNT and MWCNT-7 samples. Raman peaks at around 1358 cm^{-1}, 1590 cm^{-1}, and 2700 cm^{-1} were identified and assigned to the D-band, G-band, and 2D(G^0)-band of carbon structure (Ferrari and Basko, 2013). The intensity ratio of the defect-derived D-band to the G-band (ID/IG), an indicator of the structural integrity of the graphitic carbon lattice, was calculated based on Raman peak fitting results. A D-band to G-band intensity ratio of 0.132 was obtained for MWCNT-7, while the ND-MWCNT had a ratio of 1.440, indicating significant structural disorder induced in the graphitic carbon lattice of the ND-MWCNT due to nitrogen doping (Fig. 3).

XRD was performed to study the crystallinity condition of the MWCNT. The strong diffraction peaks at 26.3° and 42.5° were assigned to the (0 0 2) and (1 0 0) diffractions of the graphitic lattice of the MWCNT (Zhao et al., 2014). The full width at half maximum (FWHM) values of the (0 0 2) peak in MWCNT-7 and ND-MWCNT spectra were 0.91° and 1.21°, respectively. Compared to MWCNT-7, the ND-MWCNT had a broader (0 0 2) peak with lower intensity, indicating a decrease of graphene crystallinity due to nitrogen doping induced structural damage (Fig. 4).

3.3. ND-MWCNT and MWCNT-7 exposure alters SAEC proliferation

An MTS assay was carried out to determine the effects of ND-MWCNT and MWCNT-7 on SAEC proliferation. SAEC were treated with DM or 0.12, 1.2, 12, and 120 mg/ml of ND-MWCNT or MWCNT-7 for 24 h. SAEC treated with 0.12, 1.2, and 12 mg/ml ND-MWCNT exhibited a trend toward increased proliferation, which decreased at 120 mg/ml when compared to DM. Treatment of SAEC with MWCNT-7 at 0.12 mg/ml significantly increased proliferation compared to DM and 0.12 mg/mL ND-MWCNT, while treatment with 1.2 mg/ml and 12 mg/ml exhibited a lessened proliferative effect compared to DM. At 120 mg/ml, MWCNT-7 significantly decreased proliferation below that of DM (Fig. 5). In summary, MWCNT-7 significantly enhanced epithelial cell proliferation at a lower dose than ND-MWCNT. Additionally, a high dose of 120 mg/mL of MWCNT-7 was cytotoxic to the SAEC, while ND-MWCNT was not. Therefore, MWCNT-7 appear more potent in inducing proliferation and cytotoxicity than ND-MWCNT. A dose of 1.2 μg/ml was selected

for further studies as it was previously established as an occupationally relevant dose capable of inducing cellular effects in SAEC upon treatment with the particles studied here (Snyder-Talkington et al., 2013b,c,c). Also, no significant difference was noted between proliferation of SAEC treated with 1.2 μg/ml of ND-MWCNT or MWCNT-7.

3.4. ND-MWCNT and MWCNT-7 uptake by SAEC

SAEC were treated with DM (Fig. 6A), ND-MWCNT (Fig. 6B–D), or MWCNT-7 (Fig. 6E–G) and imaged for particle interaction and uptake through TEM. ND-MWCNT and MWCNT-7 varieties were found at the cell surface at 6 h (Fig. 6B, C or E, F, respectively), followed by internalization at 24 h (Fig. 6D or G, respectively).

3.5. ND-MWCNT and MWCNT-7 exposure induces ROS production in SAEC

Some fibers, including MWCNT-7, are capable of inducing the production of ROS upon interaction with various cell types (Apopa et al., 2009; Huerta-Garcia et al., 2014; Pichardo et al., 2012; Shi et al., 2014; Snyder-Talkington et al., 2013b). In this experiment, ND-MWCNT and MWCNT-7 were examined to determine their ability to induce ROS production in SAEC. SAEC exposed to DM (Fig. 7A), ND-MWCNT (Fig. 7B, C), or MWCNT-7 (Fig. 7D, E) were stained with DHE to assess ROS production at 6 and 24 h. ROS production peaked at 6 h and remained higher than control at 24 h in ND-MWCNT treated cells (Fig. 7B, C). MWCNT-7 appeared to induce ROS production at 6 h that resolved to baseline levels at 24 h (Fig. 7D, E). The more rapid response to MWCNT-7 is consistent with greater potency compared to ND-MWCNT.

3.6. ND-MWCNT and MWCNT-7 exposure affects SAEC cell cycle and CDK4 expression

The cell cycle, which regulates cell duplication and division, can be altered by MWCNT (Ding et al., 2005; Siegrist et al., 2014; Zhang and Yan, 2012). Here, the effects of ND-MWCNT and MWCNT-7 on the cell cycle were compared. SAEC were treated with DM, ND-MWCNT, and MWCNT-7 for 6 or 24 h prior to fixation and cell cycle analysis. Propidium iodide staining was used to examine potential ND-MWCNT and MWCNT-7-related changes to the cell cycle. Results are presented as percentage of cells in each phase in Table 2. Results indicate that MWCNT-7 induce a significant change in the percentage of cells in G2 compared to DM at 6 h, suggestive of cell cycle dysfunction. At 24 h, a significant difference in percentage of cells in G1 and G2 was noted in SAEC exposed to ND-MWCNT compared to MWCNT-7. A significant increase was noted between 6 and 24 h in G2 in ND-MWCNT exposed cells. Significant changes were noted between 6 and 24 h in G1 and S phase in MWCNT-7 exposed cells (Table 2). To gain a better understanding of a molecular basis for the cell cycle dysfunction, whole cell lysates were subjected to SDS-PAGE and probed for CDK4, a serine/threonine cyclin dependent kinase important to the G1 transition prior to synthesis of new DNA in S phase (Baker and Reddy, 2012). We observed an increase in CDK4 expression in SAEC exposed to ND-MWCNT over 6 h, followed by a decrease at 24 h, which is reflective of the propidium iodide cell cycle analysis results. CDK4 does not appear to play a role in the molecular mechanism employed by MWCNT-7 to induce cell cycle arrest, which was expected because CDK4 should not be active during G2 (Fig. 8).

3.7. ND-MWCNT and MWCNT-7 exposure induces phospho-tyrosine and phospho-threonine

The majority of cell signaling processes involve protein phosphorylation, especially signal transduction pathways and those essential to cell cycle regulation, cell differentiation, and cell maintenance (Hunter, 1995; Marshall, 1995). To better understand how ND-MWCNT and MWCNT-7 may affect these processes, general cell signaling pathways were probed using pan-phospho-tyrosine and phospho-threonine antibodies. SAEC were exposed to DM, ND-MWCNT, or MWCNT-7 over 6 or 24 h, and whole cell lysates were collected using RIPA buffer with protease and phosphatase inhibitors. Lysates were subjected to SDS-PAGE, transferred to PVDF membranes, and exposed to phospho-antibodies. Phospho-tyrosine expression increased at 6 h for MWCNT-7 exposed SAEC, suggesting a time-dependent activation of signaling pathways (Fig. 9A). Changes in phospho-threonine expression following MWCNT exposure were less obvious (Fig. 9B).

4. Discussion

Although MWCNT have been in production for over twenty years, functionalization offers an avenue to increase their dispersibility and industrial applications across a variety of fields. Surface functionalizations and substitution reactions (with nitrogen or boron, as examples) to the carbon lattice may increase nanotube reactivity at sites of curvature and breaks in the lattice (Kuzmany et al., 2004; Meier et al., 2008). The increase in porosity greatly increases the surface area (and therefore, reactive surface) of ND-MWCNT, which could have interesting implications for biocompatibility (Meier et al., 2008). Nitrogen functionalization (or “doping”) of CNT has been shown to significantly increase the brittleness, chemical reactivity, and n-type semiconductor activity of this material (Maldonado et al., 2006). Varying amounts of nitrogen may be incorporated into the carbon lattice, disrupting sp^2 bonding and creating potential active sites for further functionalization (e.g., drug molecules) or participation in oxygen reduction reactions (Kundu et al., 2009; Maldonado et al., 2006). Nitrogen-containing functional groups, such as amines, can also be attached to the outermost layer of graphene in CNT for use in biosensors and epoxies (Arrigo et al., 2008; Deng et al., 2009; Sharma and Shukla, 2014). However, limited information is available on how functionalization of CNT with nitrogen alters their bioactivity.

Both pyridinic and pyrrolic nitrogen atoms are located at either the structural defect sites within the graphene network or at the sheet edges of the MWCNT walls. Specifically, our ND-MWCNT appear to have pyrrolic N-incorporation. The nitrogen atoms in MWCNT, especially at the outermost layer, become attraction sites for oxygen atoms and other functional groups and significantly modify MWCNT surface chemistry. The lengths of ND-MWCNT are often shorter than pristine MWCNT due to different growth kinetics, which was observed in this study. Fiber length can play a role in toxicity and longer fibers have often been shown to be more toxic than their shorter counterparts (Donaldson and Poland, 2013; Poland et al., 2008). Data from the present study suggesting that ND-MWCNT are less bioactive than pristine MWCNT are as follows: (1) in the MTS assay, MWCNT-7 enhanced epithelial cell proliferation at a 10-fold lower dose than ND-MWCNT; (2)

MWCNT-7 caused significant cytotoxicity in the MTS assay at a dose of 120 μg/ml, while ND-MWCNT did not; and (3) MWCNT-7 induced an increase in phospho-tyrosine signaling at 6 h which may be linked to signaling cascades such as the MAPK and PI3K cascades (Ray et al., 2012). Indications that ND-MWCNT may be less damaging than pristine MWCNT *in vivo* and *in vitro* have also been reported by other labs (Nel et al., 2006). Due to the inert character and agglomeration of pristine MWCNT, it is possible that the ND-MWCNT remain better dispersed *in vivo* and are therefore less likely to block the small airways in the lungs (Carrero-Sanchez et al., 2006). *In vitro*, the hydrophilic nature and surface charge of functionalized MWCNT, including ND-MWCNT, can alter their uptake and subsequent toxicity in pulmonary epithelial and macrophage cells. Previous studies have shown no significant activation of the NRLP3 inflammasome in ND-MWCNT exposed cells when compared to undoped MWCNT, making it a potentially better choice for use in industry to protect workers and the general public (Li et al., 2013). Boncel et al. (2011) studied the cytotoxicity of 3 wt.% ND-MWCNT compared to oxidized MWCNT and pristine MWCNT and suggested that ND-MWCNT are of intermediate toxicity, but less toxic than the pristine variant.

In the present study, the bioactivities of ND-MWCNT and pristine MWCNT in short-term exposure of SAEC were compared. Our data suggests that ROS could potentially initiate the bioactivity noted in our study. It has been previously shown that MWCNT-7 produce no detectable hydroxyl radical alone or in the presence of H_2O_2 from the acellular Fenton reaction and instead scavenged ROS similar to ND-MWCNT which also scavenged ROS in the acellular Fenton reaction (Porter et al., 2010; Snyder-Talkington et al., 2013b, unpublished data). This implies that the SAEC were generating ROS in response to ND-MWCNT exposure. Within the past decade, ROS has been increasingly linked to a variety of cellular functions, including growth factor activation, cytoskeletal changes, and cell cycle progression, as well as contributing to inflammation, oxidative stress, and general cell signaling (Belousov et al., 2013; Boonstra and Post, 2004; Ray et al., 2012; Verbon et al., 2012). It has previously been shown that MWCNT are capable of inducing ROS in a variety of cell types (He et al., 2011; Pacurari et al., 2012; Snyder-Talkington et al., 2013b; Ye et al., 2009). Here, we showed that ND-MWCNT are capable of inducing ROS in SAEC in a time-dependent manner. ROS are an important part of cellular immunity, act as cell signaling agents, play a role in cytoskeletal modifications and cell cycle regulation, and can lead to the development of cancer (Verbon et al., 2012). Our results suggest that ND-MWCNT induced sustained production of ROS over a 24 h period, while MWCNT-7 induced transient production of ROS at 6 h that resolved by 24 h. This difference may be due to the physicochemical properties of the particles and their ability to scavenge ROS, which has been shown to vary with nanotube composition, surface characteristics, and redox potential in acellular systems (Tsuruoka 2013a,b; Tsuruoka et al., 2015Tsuruoka 2013a,b; Tsuruoka et al., 2015 Tsuruoka et al., 2015). As suggested by Tsuruoka, surface electrons of MWCNT may be able to scavenge ROS *in vivo* through electron donation that could be limited by the ability of cells in the body to resupply electrons to MWCNT to scavenge additional ROS. When this theory is applied to our results, SAEC may be better able to resupply electrons on the surface of MWCNT-7 or MWCNT-7 may have more surface

electrons available to donate to ROS present in our cellular system over a 24 h period (Tsuruoka et al., 2015).

Although ROS can cause oxidative damage to DNA, lipids, and proteins, we believe that the sustained levels of ROS induced by ND-MWCNT treatment may be alternatively acting as a signaling molecule as proposed by Boonstra and Post (2004). ROS can influence the cell cycle through the activation of growth factor receptors and phosphorylation and ubiquitination of cell cycle regulators (Verbon et al., 2012). The cell cycle is regulated through a series of "checkpoints" mediated by cyclins and serine/threonine cyclin-dependent kinases that tightly block or promote cycling. Several recent publications have discussed functionalized MWCNT-induced cell cycle alterations. Siegrist et al. (2014) studied carboxylated MWCNTand showed that exposure of Beas2B bronchial epithelial cells with 24 μg/cm^2 MWCNT induced a significant increase in cells in S phase, suggesting a block at the G1/S checkpoint. Zhang and Yan (2012) recently showed in several cell lines that carboxylated MWCNT caused cell cycle arrest at the transition between G1/S and a slight arrest in G2 in mouse mesenchymal stem cells and human neuroblastoma cells. Our findings suggest that ND-MWCNT and MWCNT-7 may be inducing cell cycle aberrations between 6 and 24 h at G2 phase and at 6 h in G2 phase, respectively. Our findings also show that CDK4 levels distinctly vary between 6 and 24 h in SAEC exposed to ND-MWCNT or MWCNT-7, further suggesting that they may act through alternative mechanisms to alter the cell cycle. Total phospho-threonine levels are similar to CDK4 levels for each time point and exposure, suggesting that the cellular activation may be related. Phospho-tyrosine kinases are important for a variety of different cell signaling pathways including mitogen-activated protein kinase pathways, Jak/STAT pathways, and phosphotidylinoside 3-kinase (Marshall, 1995). These signaling pathways are related to cell cycle regulation, cell differentiation, cell migration, and apoptosis (Rawlings et al., 2004). Since dysregulation of these pathways has been associated with inflammation, cancer, and diabetes, our results warrant further studies of these particles' specific molecular mechanisms. Our lab has previously shown significant increases in phospho-NF-kB p65, phospho-p38, and phospho-Stat3 in human microvascular endothelial cells indirectly exposed to MWCNT-7 in an alveolar-capillary co-culture system (Snyder-Talkington et al., 2013c). Others have also shown activation of p38 MAPK in Beas2B lung epithelial cells and normal mesothelial cells in response to MWCNT exposure, which may provide direction for future work (Hirano et al., 2010; Pacurari et al., 2008).

5.Conclusions

In this study, we present the first in-depth physicochemical characterization of these ND-MWCNT, suggesting that during synthesis, nitrogen atoms were incorporated into the MWCNT, introducing structural disorder and altering their crystallinity. Our major finding is that the differences in physicochemical properties, especially disruption of the carbon crystalline lattice by incorporation of nitrogen atoms, impacts the bioactivity of MWCNT. Overall, our findings suggest that the bioactivity of ND-MWCNT in SAEC is somewhat lower than that exhibited by pristine MWCNT due to differences in physicochemical properties. The time and dose-dependent nature of observed proliferation, cytotoxicity, ROS production, cell cycle alterations, and total phospho-tyrosine and phospho-threonine-altered

proteins suggests that the physico-chemical properties of MWCNT affect their subsequent biological effects.

Acknowledgements

A.L. Mihalchik acknowledges support from the National Science Foundation through the IGERT program under grant DGE-1144676. We would also like to acknowledge use of the WVU Shared Research Facilities.

References

Apopa PL, Qian Y, Shao R, Guo NL, Schwegler-Berry D, Pacurari M, Porter D, Shi X, Vallyathan V, Castranova V, Flynn DC. Iron oxide nanoparticles induce human microvascular endothelial cell permeability through reactive oxygen species production and microtubule remodeling. Part. Fibre Toxicol. 2009; 6:1. [PubMed: 19134195]

Arrigo R, Havecker M, Schlogl R, Su DS. Dynamic surface rearrangement and thermal stability of nitrogen functional groups on carbon nanotubes. Chem. Commun. 2008:4891–4893.

Ayala P, Arenal R, Rümmeli M, Rubio A, Pichler T. The doping of carbon nanotubes with nitrogen and their potential applications. Carbon. 2010; 48:575–586.

Baker SJ, Reddy EP. CDK4: a key player in the cell cycle, development, and cancer. Genes Cancer. 2012; 3:658–669. [PubMed: 23634254]

Belousov VV, Enikolopov GN, Mishina NM. Compartmentalization of ROS-mediated signal transduction. Russ. J. Bioorg. Chem. 2013; 39:341–355.

Boncel S, Müller KH, Skepper JN, Walczak KZ, Koziol KKK. Tunable chemistry and morphology of multi-wall carbon nanotubes as a route to non-toxic, theranostic systems. Biomaterials. 2011; 32:7677–7686. [PubMed: 21764122]

Boonstra J, Post JA. Molecular events associated with reactive oxygen species and cell cycle progression in mammalian cells. Gene. 2004; 337:1–13. [PubMed: 15276197]

Carrero-Sanchez JC, Elias AL, Mancilla R, Arrellin G, Terrones H, Laclette JP, Terrones M. Biocompatibility and toxicological studies of carbon nanotubes doped with nitrogen. Nano Lett. 2006; 6:1609–1616. [PubMed: 16895344]

Deng S, Jian G, Lei J, Hu Z, Ju H. A glucose biosensor based on direct electrochemistry of glucose oxidase immobilized on nitrogen-doped carbon nanotubes. Biosens. Bioelectron. 2009; 25:373–377. [PubMed: 19683424]

Ding L, Stilwell J, Zhang T, Elboudwarej O, Jiang H, Selegue JP, Cooke PA, Gray JW, Chen FF. Molecular characterization of the cytotoxic mechanism of multiwall carbon nanotubes and nano-onions on human skin fibroblast. Nano Lett. 2005; 5:2448–2464. [PubMed: 16351195]

Donaldson K, Poland CA. Nanotoxicity: challenging the myth of nano-specific toxicity. Curr. Opin. Biotech. 2013; 24:724–734. [PubMed: 23768801]

Elías AL, Carrero-Sánchez JC, Terrones H, Endo M, Laclette JP, Terrones M. Viability studies of pure carbon- and nitrogen-doped nanotubes with Entamoeba histolytica: from amoebicidal to biocompatible structures. Small. 2007; 3:1723–1729. [PubMed: 17849378]

Ferrari AC, Basko DM. Raman spectroscopy as a versatile tool for studying the properties of graphene. Nat. Nano. 2013; 8:235–246.

Han JH, Lee EJ, Lee JH, So KP, Lee YH, Bae GN, Lee SB, Ji JH, Cho MH, Yu IJ. Monitoring multiwalled carbon nanotube exposure in carbon nanotube research facility. Inhal. Toxicol. 2008; 20:741–749. [PubMed: 18569096]

He X, Young S-H, Schwegler-Berry D, Chisholm WP, Fernback JE, Ma Q. Multiwalled carbon nanotubes induce a fibrogenic response by stimulating reactive oxygen species production activating NF-kB signaling, and promoting fibroblast-to-myofibroblast transformation. Chem. Res. Toxicol. 2011; 24:2237–2248. [PubMed: 22081859]

Hirano S, Fujitani Y, Furuyama A, Kanno S. Uptake and cytotoxic effects of multi-walled carbon nanotubes in human bronchial epithelial cells. Toxicol. Appl. Pharmacol. 2010; 249:8–15. [PubMed: 20800606]

Huerta-Garcia E, Perez-Arizti JA, Marquez-Ramirez SG, Delgado-Buenrostro NL, Chirino YI, Iglesias GG, Lopez-Marure R. Titanium dioxide nanoparticles induce strong oxidative stress and mitochondrial damage in glial cells. Free Radic. Biol. Med. 2014; 73:84–94. [PubMed: 24824983]

Hunter T. Protein kinases and phosphatases: the yin and yang of protein phosphorylation and signaling. Cell. 1995; 80:225–236. [PubMed: 7834742]

Kasai, T.; Umeda, Y.; Ohnishi, M.; Kondo, H.; Takeuchi, T.; Aiso, S.; Nishizawa, T.; Matsumoto, M.; Fukushima, S. Thirteen-week study of toxicity of fiber-like multi-walled carbon nanotubes with whole-body inhalation exposure in rats; Nanotoxicology. 2014. p. 1-10.http://informahealthcare.com/doi/full/10.3109/17435390.2014.933903.

Kundu S, Nagaiah TC, Xia W, Wang Y, Dommele SV, Bitter JH, Santa M, Grundmeier G, Bron M, Schuhmann W, Muhler M. Electrocatalytic activity and stability of nitrogen-containing carbon nanotubes in the oxygen reduction reaction. J. Phys. Chem. C. 2009; 113:14302–14310.

Kuzmany H, Kukovecz A, Simon F, Holzweber M, Kramberger C, Pichler T. Functionalization of carbon nanotubes. Synth. Met. 2004; 141:113–122.

Li R, Wang X, Ji Z, Sun B, Zhang H, Chang CH, Lin S, Meng H, Liao YP, Wang M, Li Z, Hwang AA, Song TB, Xu R, Yang Y, Zink JI, Nel AE, Xia T. Surface charge and cellular processing of covalently functionalized multiwall carbon nanotubes determine pulmonary toxicity. ACS Nano. 7. 2013:2352–2368. [PubMed: 23414138]

Maldonado S, Morin S, Stevenson KJ. Structure, composition, and chemical reactivity of carbon nanotubes by selective nitrogen doping. Carbon. 2006; 44:1429–1437.

Marshall CJ. Specificity of receptor tyrosine kinase signaling: transient versus sustained extracellular signal-regulated kinase activation. Cell. 1995; 80:179–185. [PubMed: 7834738]

Meier MS, Andrews R, Jacques D, Cassity KB, Qian D. Tearing open nitrogen-doped multiwalled carbon nanotubes. J. Mater. Chem. 2008; 18:4143.

Mercer R, Hubbs A, Scabilloni J, Wang L, Battelli L, Schwegler-Berry D, Castranova V, Porter D. Distribution and persistence of pleural penetrations by multi-walled carbon nanotubes. Part. Fibre Toxicol. 2010; 7:11. [PubMed: 20420656]

Mercer R, Hubbs A, Scabilloni J, Wang L, Battelli L, Friend S, Castranova V, Porter D. Pulmonary fibrotic response to aspiration of multi-walled carbon nanotubes. Part. Fibre Toxicol. 2011; 8:21. [PubMed: 21781304]

Mercer RR, Scabilloni JF, Hubbs AF, Battelli LA, McKinney W, Friend S, Wolfarth MG, Andrew M, Castranova V, Porter DW. Distribution and fibrotic response following inhalation exposure to multi-walled carbon nanotubes. Part. Fibre Toxicol. 2013; 10:33. [PubMed: 23895460]

Mishra A, Rojanasakul Y, Chen BT, Castranova V, Mercer RR, Wang L. Assessment of pulmonary fibrogenic potential of multiwalled carbon nanotubes in human lung cells. J. Nanomater. Mar.2012 2012 :1–11.

National Institute for Occupational Safety and Health. Occupational Exposure to Carbon Nanotubes and Nanofibers, Current Intelligence Bulletin. 2013; 65

Nel A, Xia T, Mädler L, Li N. Toxic potential of materials at the nanolevel. Science. 2006; 311:622–627. [PubMed: 16456071]

Oberlin A, Endo M, Koyama T. Filamentous growth of carbon through benzene decomposition. J. Cryst. Growth. 1976; 32:335–349.

Pacurari M, Yin X, Ding M, Leonard S, Schwegler-Berry D, Ducatman B, Chirila M, Endo M, Castranova V, Vallyathan V. Oxidative and molecular interactions of multi-wall carbon nanotubes (MWCNT) in normal and malignant human mesothelial cells. Nanotoxicology. 2008; 2:155–170.

Pacurari M, Qian Y, Porter DW, Wolfarth M, Wan Y, Luo D, Ding M, Castranova V, Guo NL. Multi-walled carbon nanotube-induced gene expression in the mouse lung: association with lung pathology. Toxicol. Appl. Pharmacol. 2011; 255:18–31. [PubMed: 21624382]

Pacurari M, Qian Y, Fu W, Schwegler-Berry D, Ding M, Castranova V, Guo NL. Cell permeability, migration, and reactive oxygen species induced by multiwalled carbon nanotubes in human microvascular endothelial cells. J. Toxicol. Environ. Health A. 2012; 75:112–128. [PubMed: 22129238]

Piao CQ, Liu L, Zhao YL, Balajee AS, Suzuki M, Hei TK. Immortalization of human small airway epithelial cells by ectopic expression of telomerase. Carcinogenesis. 2005; 26:725–731. [PubMed: 15677631]

Pichardo S, Gutierrez-Praena D, Puerto M, Sanchez E, Grilo A, Camean AM, Jos A. Oxidative stress responses to carboxylic acid functionalized single wall carbon nanotubes on the human intestinal cell line Caco-2. Toxicol. 2012; 26:672–677. In Vitro.

Poland CA, Duffin R, Kinloch I, Maynard A, Wallace WAH, Seaton A, Stone V, Brown S, MacNee W, Donaldson K. Carbon nanotubes introduced into the abdominal cavity of mice show asbestos-like pathogenicity in a pilot study. Nat. Nano. 2008; 3:423–428.

Porter D, Sriram K, Wolfarth M, Jefferson A, Schwegler-Berry D, Andrew ME, Castranova V. A biocompatible medium for nanoparticle dispersion. Nanotoxicology. 2008; 2:144–154.

Porter D, Hubbs A, Mercer R, Wu N, Wolfarth M, Sriram K, Leonard S, Battelli L, Schwegler-Berry D, Friend S, Andrew M, Chen B, Tsuruoka S, Endo M, Castranova V. Mouse pulmonary dose- and time course-responses induced by exposure to multi-walled carbon nanotubes. Toxicology. 2010; 269:136–147. [PubMed: 19857541]

Porter D, Hubbs A, Chen B, McKinney W, Mercer R, Wolfarth M, Battelli L, Wu N, Sriram K, Leonard S, Andrew M, Willard P, Tsuroka S, Endo M, Tsukada T, Munekane F, Frazer D, Castranova V. Acute pulmonary dose-responses to inhaled multi-walled carbon nanotubes. Nanotoxicology. 2013; 7(7):1179–1194. [PubMed: 22881873]

Qian Y, Ducatman A, Ward R, Leonard S, Bukowski V, Lan Guo N, Shi X, Vallyathan V, Castranova V. Perfluorooctane sulfonate (PFOS) induces reactive oxygen species (ROS) production in human microvascular endothelial cells: role in endothelial permeability. J. Toxicol. Environ. Health A. 2010; 73:819–836. [PubMed: 20391123]

Rawlings JS, Rosler KM, Harrison DA. The JAK/STAT signaling pathway. J. Cell Sci. 2004; 117:1281–1283. [PubMed: 15020666]

Ray PD, Huang B-W, Tsuji Y. Reactive oxygen species (ROS) homeostasis and redox regulation in cellular signaling. Cell Signal. 2012; 24:981–990. [PubMed: 22286106]

Riddick, T. Control of Colloid Stability Through Zeta Potential: With a Closing Chapter on Its Relationship to Cardiovascular Disease. Livingston Publishing Company; 1968.

Seran C, Hyungu I, Jooheon K. The thermal conductivity of embedded nano-aluminum nitride-doped multi-walled carbon nanotubes in epoxy composites containing micro-aluminum nitride particles. Nanotechnology. 2012; 23:6.

Sharifi T, Nitze F, Barzegar HR, Tai C-W, Mazurkiewicz M, Malolepszy A, Stobinski L, Wâgberg T. Nitrogen doped multi walled carbon nanotubes produced by CVD-correlating XPS and Raman spectroscopy for the study of nitrogen inclusion. Carbon. 2012; 50:3535–3541.

Sharma K, Shukla M. Molecular modeling of the mechanical behavior of carbon fiber-amine functionalized multiwall carbon nanotube/epoxy composites. New Carbon Mater. 2014; 29:132–142.

Shi J, Sun X, Lin Y, Zou X, Li Z, Liao Y, Du M, Zhang H. Endothelial cell injury and dysfunction induced by silver nanoparticles through oxidative stress via IKK/NF-kB pathways. Biomaterials. 2014; 35(24):6657–6666. [PubMed: 24818879]

Siegrist KJ, Reynolds SH, Kashon ML, Lowry DT, Dong C, Hubbs AF, Young SH, Salisbury JL, Porter DW, Benkovic SA, McCawley M, Keane MJ, Mastovich JT, Bunker KL, Cena LG, Sparrow MC, Sturgeon JL, Dinu CZ, Sargent LM. Genotoxicity of multi-walled carbon nanotubes at occupationally relevant doses. Part. Fibre Toxicol. 2014; 11:6. [PubMed: 24479647]

Snyder-Talkington BN, Qian Y, Castranova V, Guo NL. New perspectives for in vitro risk assessment of multi-walled carbon nanotubes: application of coculture and bioinformatics. J. Toxicol. Environ. Health B Crit. Rev. 2012; 15(7):49–468.

Snyder-Talkington BN, Dymacek J, Porter DW, Wolfarth MG, Mercer RR, Pacurari M, Denvir J, Castranova V, Qian Y, Guo NL. System-based identification of toxicity pathways associated with multi-walled carbon nanotube-induced pathological responses. Toxicol. Appl. Pharmacol. 2013a; 272:476–489. [PubMed: 23845593]

Snyder-Talkington BN, Pacurari M, Dong C, Leonard SS, Schwegler-Berry D, Castranova V, Qian Y, Guo NL. Systematic analysis of multiwalled carbon nanotube-induced cellular signaling and gene

expression in human small airway epithelial cells. Toxicol. Sci. 2013b; 133:79–89. [PubMed: 23377615]

Snyder-Talkington BN, Schwegler-Berry D, Castranova V, Qian Y, Guo NL. Multi-walled carbon nanotubes induce human microvascular endothelial cellular effects in an alveolar-capillary co-culture with small airway epithelial cells. Part. Fibre Toxicol. 2013c; 10:35. [PubMed: 23903001]

Terrones M, Ajayan PM, Banhart F, Blase X, Carroll DL, Charlier JC, Czerw R, Foley B, Grobert N, Kamalakaran R, Kohler-Redlich P, Rühle M, Seeger T, Terrones H. N-doping and coalescence of carbon nanotubes: synthesis and electronic properties. Appl. Phys. 2002; 74:355–361.

Tsuruoka KT, Koyama K, Noguchi T, Endo M, Tristan F, Terrones M, Matsumoto H, Saito N, Usui Y, Porter DW, Castranova V. ROS evaluation for a series of CNTs and their derivatives using an ESR method with DMPO. J. Phys. Conf. Ser. 2013a; 429

Tsuruoka S, Cassee FR, Castranova V. A new approach to design safe CNTs with an understanding of redox potential. Part. Fibre Toxicol. 2013b; 10:44. [PubMed: 24004820]

Tsuruoka S, Matsumoto H, Koyama K, Akiba E, Yanagisawa T, Cassee FR, Saito N, Usui Y, obayashi S, Porter DW, Castranova V, Endo M. Radical scavenging reaction kinetics with multiwalled carbon nanotubes. Carbon. 2015; 83:232–239.

Verbon EH, Post JA, Boonstra J. The influence of reactive oxygen species on cell cycle progression in mammalian cells. Gene. 2012; 511:1–6. [PubMed: 22981713]

Wang L, Stueckle TA, Mishra A, Derk R, Meighan T, Castranova V, Rojanasakul Y. Neoplastic-like transformation effect of single-walled and multi-walled carbon nanotubes compared to asbestos on human lung small airway epithelial cells. Nanotoxicology. 2014; 8:485–507. [PubMed: 23634900]

Ye SF, Wu YH, Hou ZQ, Zhang QQ. ROS and NF-kB are involved in upregulation of IL-8 in A549 cells exposed to multi-walled carbon nanotubes. Biochem. Biophys. Res. Commun. 2009; 379:643–648. [PubMed: 19121628]

Zhang C, Hao R, Liao H, Hou Y. Synthesis of amino-functionalized graphene as metal-free catalyst and exploration of the roles of various nitrogen states in oxygen reduction reaction. Nano Energy. 2013; 2:88–97.

Zhang Y, Yan B. Cell cycle regulation by carboxylated multiwalled carbon nanotubes through p53-independent induction of p21 under the control of the BMP signaling pathway. Chem. Res. Toxicol. 2012; 25:1212–1221. [PubMed: 22428663]

Zhao ML, Li DJ, Yuan L, Yue YC, Liu H, Sun X. Differences in cytocompatibility and hemocompatibility between carbon nanotubes and nitrogen-doped carbon nanotubes. Carbon. 2011; 49:3125–3133.

Zhao T, Hou C, Zhang H, Zhu R, She S, Wang J, Li T, Liu Z, Wei B. Electromagnetic wave absorbing properties of amorphous carbon nanotubes. Sci. Rep. 2014; 4

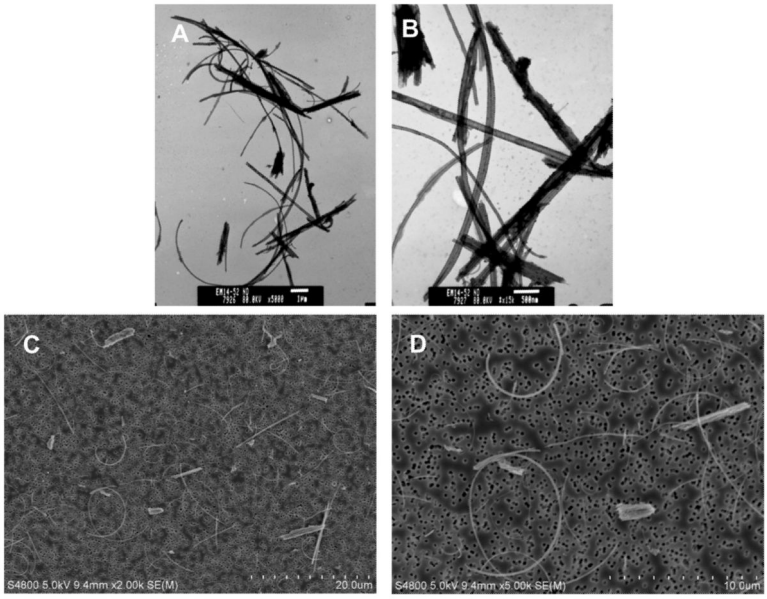

Fig. 1.

TEM of ND-MWCNT at 5000x (A) and 15000x (B) and field emission scanning electron micrographs of ND-MWCNT at 2000x (C) and 5000x (D).

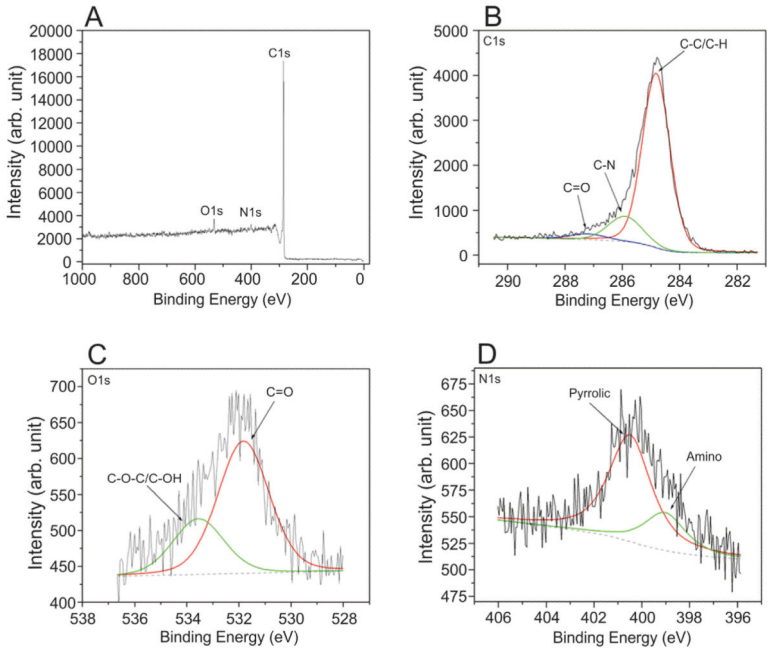

Fig. 2.

X-ray photoelectron spectroscopy survey scan spectrum of ND-MWCNT sample (A), high resolution X-ray photoelectron spectroscopy spectra for carbon (B), nitrogen (C), and oxygen elements (D).

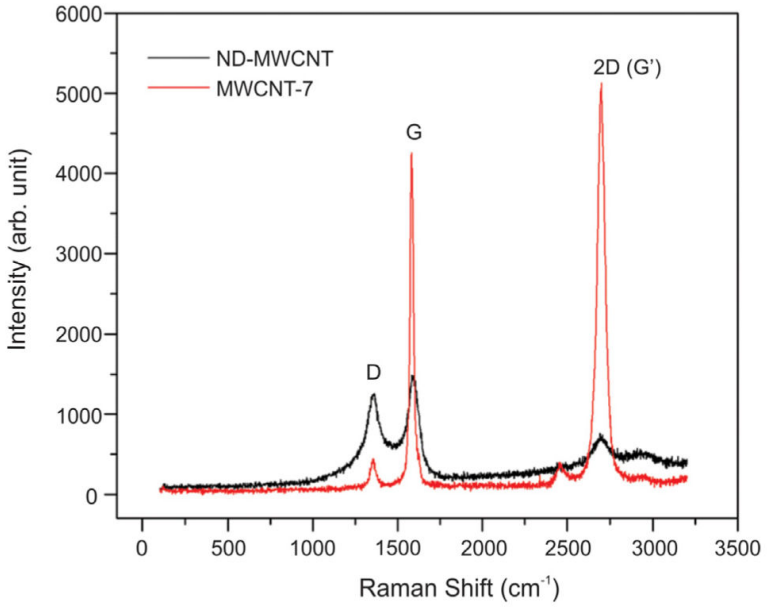

Fig. 3.
Raman spectra of ND-MWCNT and MWCNT-7 samples.

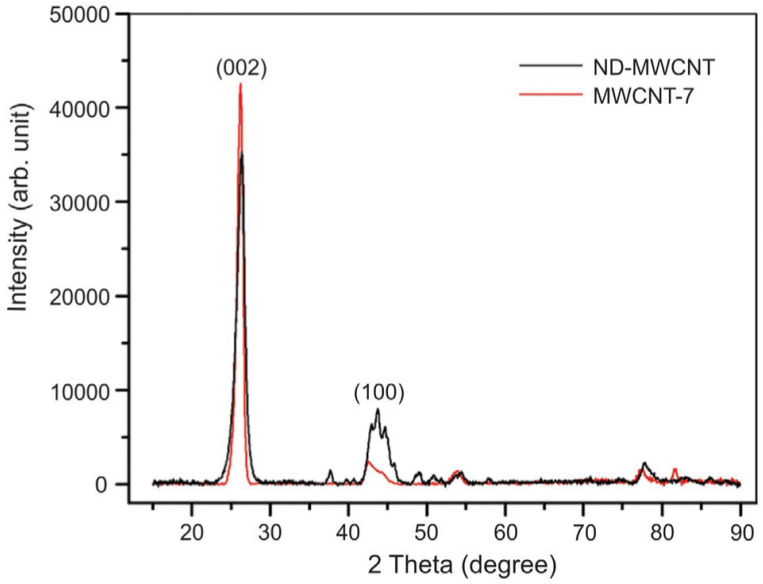

Fig. 4.
X-ray diffraction spectra of ND-MWCNT and MWCNT-7 samples.

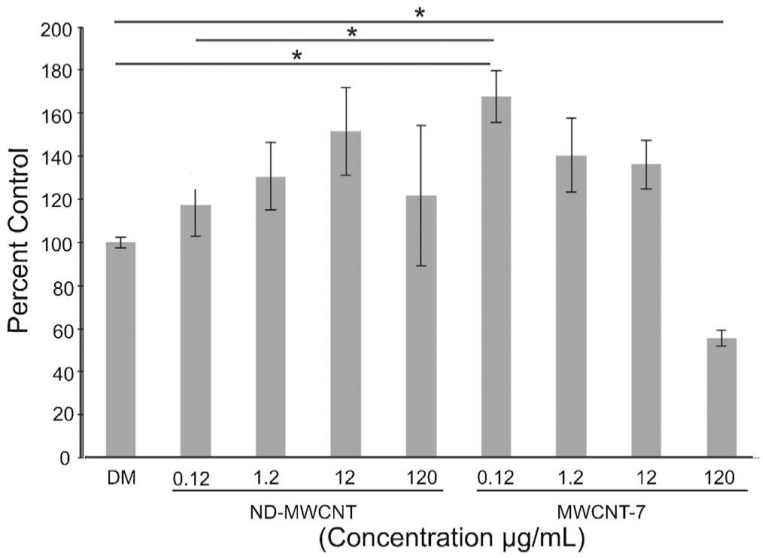

Fig. 5.

SAEC were treated with varying concentrations of DM, ND-MWCNT, or MWCNT-7 for a 24 h period. CellTiter 96® Aqueous One Solution was added 4 h prior to end of exposure and absorbance was measured at 490 nm. Results indicate that MWCNT-7 induces a significant increase in cell proliferation at 0.12 μg/ml compared to DM and ND-MWCNT at 1.2 μg/ml and decrease at 120 μg/ml compared to DM. * $p \leq 0.05$.

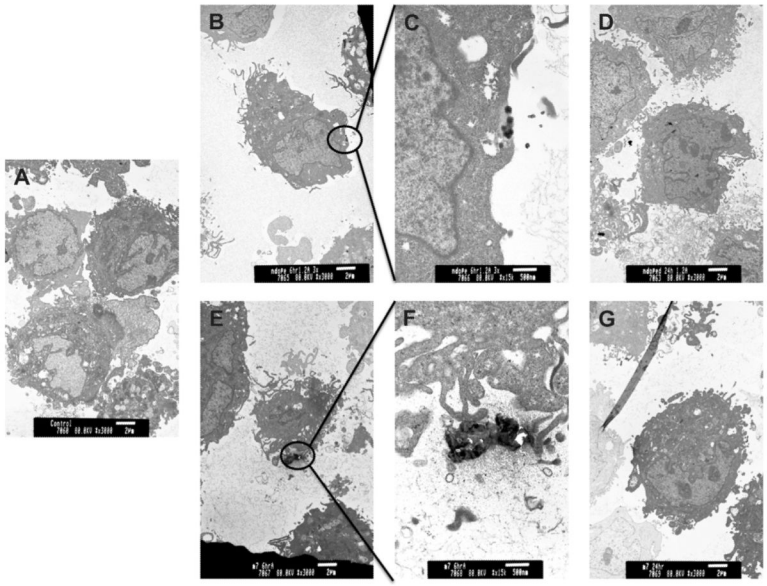

Fig. 6.

TEM images of SAEC treated with (A) 1.2 μg/ml DM, (B–D) ND-MWCNT, or (E–G) MWCNT-7 for 6 h (column 2, 3) or 24 h (column 4).

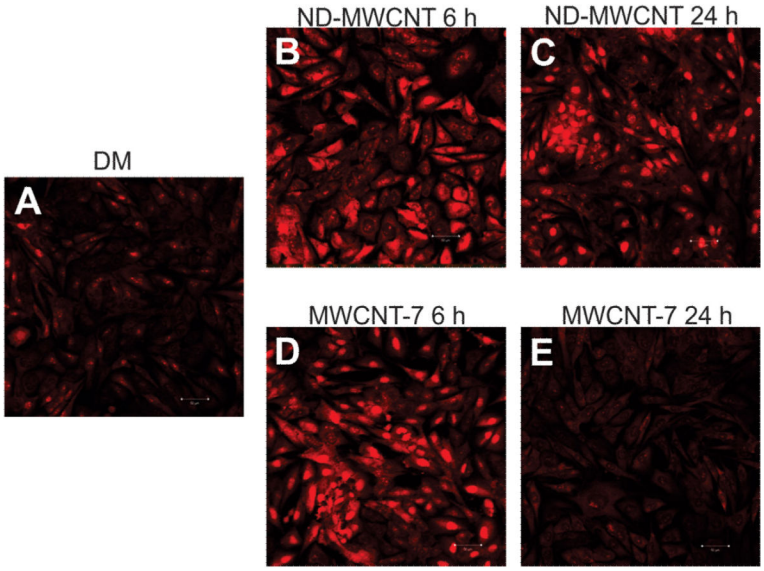

Fig. 7.

Confocal images of SAEC treated with 1.2 μg/ml DM (A), ND-MWCNT (B, C), or MWCNT-7 (D, E) over 6 (B, D) or 24 h (C, E) followed by staining with DHE for presence of ROS.

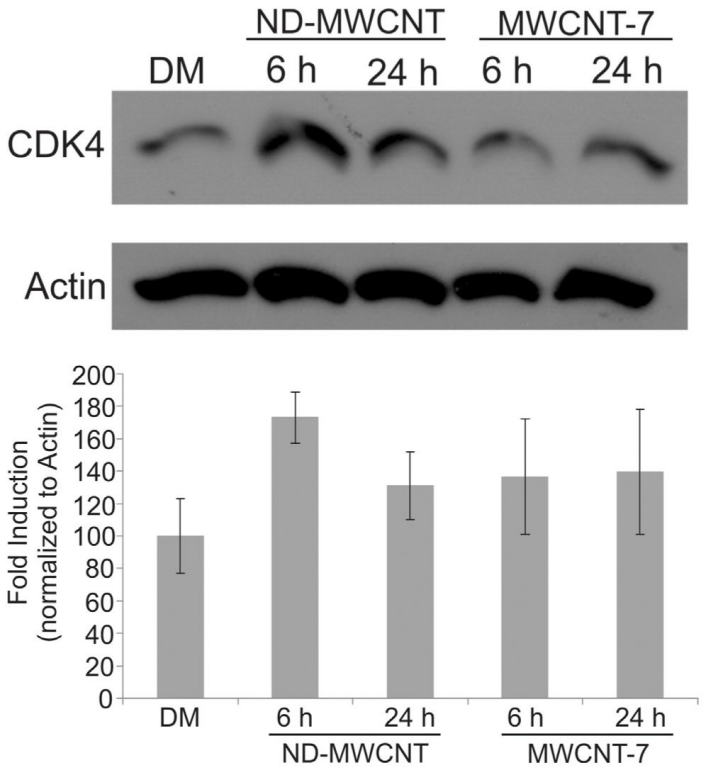

Fig. 8.

SAEC were grown to subconfluence and treated with 1.2 μg/ml DM, ND-MWCNT, or MWCNT-7 over 6 or 24 h. Whole cell lysates were resolved by SDS-PAGE on ten percent gels and probed for CDK4, which appeared to be increased at 6 h in ND-MWCNT-treated SAEC. β-actin was used as a loading control. Densitometry results (n = 3) are presented below the blot.

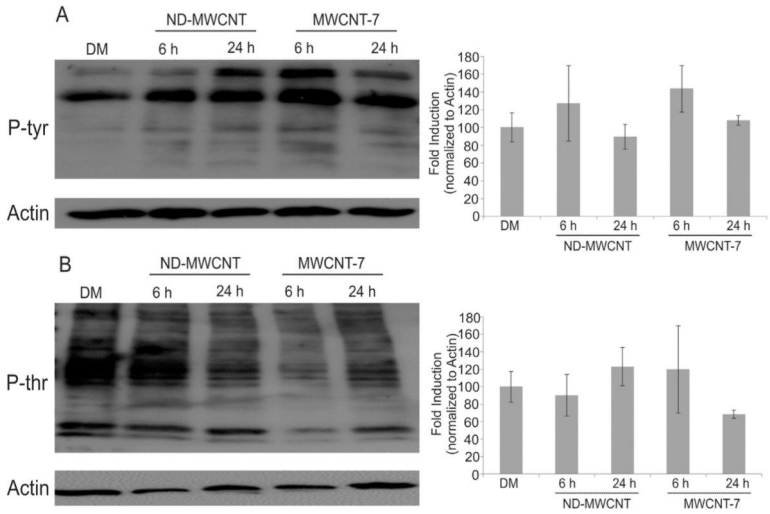

Fig. 9.

SAEC were treated with 1.2 μg/ml DM, ND-MWCNT, or MWCNT-7 over 6 or 24 h. Whole cell lysates were resolved by SDS-PAGE on ten percent gels and probed for phospho-tyrosine (A) or phospho-threonine (B) indicating that cell signaling response may be time and particle dependent. β-actin was used as a loading control. Densitometry results (n = 3) are presented to the right of each blot.

Table 1

Zeta potentials of ND-MWCNT and MWCNT-7 in PBS (pH 7.2) and serum-free media (pH 7.6).

	Dimensions		**Zeta potential (mV)**	**(Mean ± standard error)**
ND-MWCNT	Length (μm)	5.28 ± 2.07	PBS (pH 7.2)	− 13.9 ± 0.483
	Width (nm)	79.7 ± 19.4	Serum-free media (pH 7.6)	− 12.9 ± 0.835
MWCNT-7	Length (μm)	3.86 (GSD 1.94)	PBS (pH 7.2)	− 15.8 ± 0.450
	Width (nm)	49 ± 13.4 nm	Serum-free media (pH 7.6)	− 12.2 ± 0.283

Table 2

SAEC were grown to subconfluence and treated with 1.2 μg/ml DM, ND-MWCNT, or MWCNT-7 over 6 or 24 h prior to ethanol fixation, staining with propidium iodide, and assessment using a FACS SR instrument. Results presented indicate an increased percentage of cells in G2 compared to DM and significant changes between 6 and 24 h in G1 and S phase in MWCNT-7 exposed SAEC, while ND-MWCNT induced significant changes between 6 and 24 h in G2. Significant changes are also noted at 24 h between MWCNT-7 and ND-MWCNT exposed SAEC at G1 and G2.

Treatment	%G1 ± std error	%S ± std error	%G2 ± std error
MWCNT-7 DM	79.3 ± 2.03	14.4 ± 1.70	3.37 ± 0.232
MWCNT-7 6 h	77.8 ± 0.492*	15.1 ± 0.325*	4.25 ± 0.307*
MWCNT-7 24 h	79.6 ± 0.587*	14.2 ± 0.152*	3.80 ± 0.344*
ND-MWCNT DM	76.1 ± 2.13	16.1 ± 1.9	4.16 ± 0.091
ND-MWCNT 6 h	79.1 ± 2.59	14.4 ± 2.06	3.45 ± 0.350*
ND-MWCNT 24 h	76.2 ± 0.848*	16.6 ± 0.848	4.67 ± 0.222*

* $p \leq 0.05$.